ROYAL SOCIETY OF CHEMISTRY

Check for updates

All polymeric conductive strain sensors with excellent skin adhesion, recovery, and long-term stability prepared from an anion–zwitterion based hydrogel†

Goeun Lee,[ab] Hyunsu Seo,[a] Daewoo Kim, [b] Seunghan Shin[ac] and Kiok Kwon [*a]

Developing a high-performing hydrogel with long-lasting skin adhesion, high ionic conductivity, mechanical stability, and fatigue resistance is a crucial issue in the field of wearable electronic devices. Because of their weak mechanical properties, zwitterion-based hydrogels are not suitable for application in wearable strain sensors despite their excellent adhesion to the skin. In this study, a hydrogel of polymer without additive was prepared by using polymerizable monomers consisting of zwitterionic 3-(1-vinyl-3-imidazolio)propanesulfonate (VIPS), anionic 2-acrylamido-2-methyl-1-propanesulfonic acid sodium salt (AMPSs), and acrylamide (AAm); the hydrogel is abbreviated as P(AMPSs/VIPS-*co*-AAm). The P(AMPSs/VIPS-*co*-AAm) hydrogel shows exceptional adhesive strength, reaching up to 26.29 kPa (lap shear to porcine skin) and high stretchability (with a fracture strain of 1282% and stress of 40 kPa). The high polarity of the AMPSs/VIPS pair improves the interfacial adhesion to the skin, the internal cohesion and recovery tendency. Unique structural characteristics of the hydrogel impart excellent fatigue resistance, network toughening, and electrical stability after multiple deformations. Thus, the prepared hydrogel has an ionic conductivity (0.51 S m^{-1}), strain sensitivity, and long-term skin adhesion, and it demonstrates potential to be applied for wearable strain sensors.

1. Introduction

A hydrogel, which is composed of a three-dimensional network structure and water, has numerous advantages when it is used as an adhesive. Its exceptional properties such as structural similarity to skin tissue and flexibility makes it a promising material for wearable-device applications.[1] A multifunctional hydrogel with high ionic conductivity, tight skin adhesion, stretchability, physical toughness, and low hysteresis must be developed to meet the escalating requirements for strain sensor application.[2] For the accurate transmission of body movement to electrical signals, securing conformal contact of the hydrogel to the skin for a long duration is crucial. Zwitterionic molecules with both positive and negative charges in one molecule have a high dipole moment.[3] The ion–dipole or dipole–dipole interaction, which is caused by the strong dual polarity of zwitterionic molecules, endows the zwitterionic hydrogel tough

bonding to various surfaces, especially to skin.[4] Because of these characteristics, zwitterion hydrogels have been studied as a suitable material for skin adhesion.[5]

However, zwitterion hydrogels lack sufficient mechanical properties because of the electrostatic repulsion between charged monomers in the polymerization process. To date, numerous efforts have been made toward increasing the toughness of zwitterion hydrogels by incorporating other tough polymer networks[6,7] or nanofillers.[8–10] For example, Xinije Pei *et al.*[8] reported that the incorporation of dopamine-modified LAPONITE® XLG into sulfobetaine methacrylate (SBMA)-based zwitterion hydrogels simultaneously enhanced the mechanic properties and increased the skin adhesion strength to 22 kPa. Yang *et al.*[9] incorporated cellulose nanocrystals into SBMA-based hydrogels to form physical cross-linking, thereby improving the mechanical properties of hydrogels. However, the hydrogel prepared by the above-mentioned procedures has structural heterogeneity between the main polymer network and incorporated fillers or other polymers. The non-uniformity of the internal structure of the hydrogel may cause structural instability of the hydrogel during repeated deformation and long-term use and may make maintaining stable characteristics such as ionic conductivity and recovery capability difficult.[11]

This study introduces an AMPSs/VIPS pair derived all polymeric hydrogel (labeled P(AMPSs/VIPS-*co*-AAm)) having

aGreen and Sustainable Materials R&D Department, Korea Institute of Industrial Technology (KITECH), Republic of Korea. E-mail: kioks@kitech.re.kr

bDepartment of Chemical and Biomolecular Engineering, Yonsei University (YU), Seodaemun-gu, Seoul, 03722, Republic of Korea

cDepartment of Green Process and System Engineering, Korea University of Science & Technology (UST), Cheonan, Chungnam 31056, Republic of Korea

† Electronic supplementary information (ESI) available. See DOI: https://doi.org/10.1039/d2ra07990a

multifunctionality with a high ionic conductivity as well as excellent skin adhesion, stretchability, strain sensitivity, and hysteresis resistance. We rationally designed a hydrogel structure to secure mechanical toughness while taking advantage of interfacial adhesiveness of zwitterion hydrogel. This high-performance hydrogel is prepared by photopolymerization of AMPSs/VIPSs pair and acrylamide (AAm) in the presence of methylene bis-acrylamide (MBAA). We focus on the use of AMPSs/VIPS pair and incorporation of AAm. It is reported that imidazolium cations of VIPS tend to combine with the anionic AMPSs, and the resulting strong ionic bond enhance the mechanical strength of hydrogel *via* working as reversible secondary cross-linking points.[6,12] As a result, we anticipated that the high polarity of the AMPSs/VIPS pair not only improved the interfacial adhesion through the ion–dipole or dipole–dipole interaction with skin surface, but also enhance the internal cohesion. In addition, AAm was copolymerized to helps the hydrogel become physically robust through formation of a longer polymer chain and hydrogen bond formation.

As a result, the P(AMPSs/VIPS-*co*-AAm) hydrogel, prepared from all polymerizable monomers without use of any additives, shows advantageous performances such as outstanding skin adhesion, ion conductivity, mechanical toughness, and fatigue resistance. Especially, P(AMPSs/VIPS-*co*-AAm) hydrogel with an optimal formulation has an adhesion strength of up to 26.29 kPa to porcine skin, these values are comparable to the highest values related to skin adhesion of previously reported zwitterion-based hydrogels.[8–10,13–15] Moreover, it is confirmed that the prepared hydrogel retains excellent adhesion to the skin even after several hours of dehydration, and it effectively functions as a strain sensor for accurately detecting body motions while maintaining direct adhesion to the body. The hydrogel can be stretched by 1282% with fracture stress of 40 kPa. Moreover, the structural stability and excellent recovery tendency attributed to the formation of secondary cross-linking sites such as ionic interaction and hydrogen bonding allow the P(AMPSs/VIPS-*co*-AAm) hydrogel to have excellent durability against repeated deformation and long-term use. On the basis of these advantageous characteristics, the P(AMPSs/VIPS-*co*-AAm) hydrogel demonstrates potential to be applied to wearable strain-sensor applications wherein excellent skin adhesion and recovery tendency are required.

2. Experimental methods

2.1. Materials

Acrylamide (AAm, ≥99%), 2-acrylamido-2-methyl-1-propanesulfonic acid sodium salt solution (AMPSs, 50 wt% in H_2O), 1-vinylimidazole (≥99%), 1,3-propanesultone (98%), acetonitrile (ACS reagent, ≥99.5%), methylene bis-acrylamide (MBAA, ≥99%), 2-hydroxy-4-(2-hydroxyethoxy)-2-methylpropiophenone (I2959, 98%), and potassium bromide (KBr, Fourier transform infrared (FTIR) grade, ≥99%) were purchased from Sigma-Aldrich.

2.2. Synthesis of 3-(1-vinyl-3-imidazolio)propanesulfonate (VIPS)

VIPS monomer was synthesized following the method reported previously.[16] 1-Vinylimidazole (0.22 mol, 20 mL) was dissolved in 100 mL of acetonitrile. An equimolar amount of 1,3-propanesultone (0.22 mol, 22 mL) was then added dropwise to the 1-vinylimidazole solution. To remove any reaction inhibitors such as oxygen and water, the mixture flask was sealed with a septum and bubbled with nitrogen for 20 minutes. The mixture was then stirred for 1 day at 34 °C. After the reaction, the VIPS was formed as a white precipitate with 80% yield and was then washed with diethyl ether at least three times. Finally, the product was then dried in a vacuum by holding for 48 hours at room temperature. The purity of VIPS was ascertained by using [1]H Nuclear Magnetic Resonance (NMR, 300 MHz, DMSO-d_6, δ): 9.70 (s, 1H), 8.20 (s, 1H), 7.95 (s, 1H), 7.32 (t, 1H), 5.95 (d, 1H), 5.42 (d, 1H), 4.37 (t, 2H), 2.62 (t, 2H), 2.15 (m, 2H).

2.3. Fabrication of P(AMPSs/VIPS-*co*-AAm) hydrogel

The P(AMPSs/VIPS-*co*-AAm) hydrogel was prepared by free-radical polymerization of VIPS, AMPSs, and AAm monomers in deionized water; the formulations are listed in Table S1.† Equimolar amounts of VIPS (6 g), AMPSs (12 g), and AAm (3.99 g) were dissolved in deionized water (17 mL) at room temperature. Chemical cross-linker MBAA (1.30 g) solution and photoinitiator I2959 (0.13 g) were then added to the mixed solution and stirred for approximately 30 minutes until they were completely dissolved. Subsequently, the precursor solution was transferred into silicon molds and irradiated using a 15 W, 365 nm UV lamp (Vilber, VL-215.LC) for 2 hours at room temperature. P(AMPSs-*co*-AAM) hydrogels were synthesized *via* the same method.

2.4. Characterization

2.4.1. Surface morphology. The surface morphology of the hydrogels could be determined by scanning electron microscopy (SEM, JSM-6701F, Jeol). After moisture from the hydrogel was removed using liquid nitrogen, the hydrogel was fractured. Next, the frozen samples were freeze-dried in a lyophilizer (Eyela, FDU-1200) for 3 days. The fractured surfaces were coated with platinum for 45 seconds and observed by SEM.

2.4.2. Thermal analysis. A differential scanning calorimetry (DSC) instrument, DSC 8500 (PerkinElmer), was used to record the melting point. Approximately 5 mg of the sample was put in an aluminum pan and tightly sealed. DSC was performed at a scan rate of 10 °C min^{-1} under a flow of nitrogen.

2.4.3. FTIR analysis. FTIR spectra of the P(AMPSs/VIPS-*co*-AAm) dry hydrogel sample and each monomer powder (AMPSs, VIPS, AAm) were analyzed by producing a KBr pellet (with a mixture/KBr ratio of 1 : 100). The FTIR spectra were obtained in the transmission measurement within a scanning range of 4500–600 cm^{-1} at a resolution of 2 cm^{-1} and in 16 scans.

2.4.4. Adhesion measurements. The 90° peeling test was performed using a SurTA Extra 2A System (Chemilab). The hydrogel sample was a rectangle of size 15 mm × 80 mm × 30 mm (WHD). The test was performed after waiting for 15 minutes such that the sample adhered well to the interface of steel, glass, and the pig skin separately. The mean and standard deviation values of at least three measurements were derived.

Lap shear tests were conducted using a universal testing machine (SurTA Extra 2A System, Chemilab). A P(AMPSs/VIPS-co-AAm) hydrogel sample was cut to a size of 15 mm × 15 mm × 3 mm (WHD) and sandwiched between pig skin sheets (size: 15 mm × 30 mm × 1.5 mm) with an adhesion area of 15 mm × 15 mm. The adhered hydrogel sample was measured after approximately 10 minutes to ensure good contact. The lap shear test was performed at a rate of 100 mm min^{-1} at room temperature. At least three measurements were obtained, and the results are reported as mean ± standard deviation.

2.4.5. Mechanical testing. Tensile tests were conducted on the hydrogel samples cut into dumbbell-shaped ASTM D638-type V specimens (overall length: 3.18 mm; gauge length (I_0): 9.53 mm; thickness: 3 mm). The tests were performed at a rate of 100 mm min^{-1} on at least three dumbbell-shaped specimens, and the results were recorded as mean ± standard deviation.

Cyclic loading–unloading tensile tests were performed up to a strain of 500%. The hysteresis energy (U_{hys}) was calculated as follows:

$$U_{hys} = \int_{loading}^{\sigma} \Delta\varepsilon - \int_{unloading}^{\sigma} \Delta\varepsilon$$

2.4.6. Electrical property measurements. The ionic conductivity of the hydrogels was determined by impedance spectroscopy through an electrochemical workstation (Autolab, AUT51733) at a frequency range of 1×10^{-1} to 1×10^{2}. In addition, the ionic conductivity (σ, S m^{-1}) was calculated as follows:

$$\sigma = L/(R \times S)$$

where L is the thickness of the hydrogel, R is the resistance, and S is the contact area of the hydrogel.

The changes in the real-time relative resistance were recorded by a digital multimeter (Owon B35T) under a given strain of the hydrogel. The resistance change was measured by winding a copper wire around the end of the hydrogel attached to the skin and connecting it to the multimeter. The relative resistance change was calculated as follows:

$$\frac{\Delta R}{R_0} = \left\{ \frac{R - R_0}{R_0} \right\} \times 100\%$$

where R_0 and R are the original and stretched resistances, respectively.

The gauge factor is defined as GF $= (\Delta R/R_0)/\varepsilon$, where ε is the strain of the hydrogel.

3. Results and discussion

3.1. Preparation of the all polymeric P(AMPSs/VIPS-co-AAm) hydrogel

The overall preparation process and structure of the P(AMPSs/VIPS-co-AAm) hydrogel are illustrated in Fig. 1. A precursor solution consisting of ionic AMPSs and zwitterionic VIPS, AAm, and MBAA was polymerized by UV irradiation to form a hydrogel network. Imidazolium cations of VIPS tend to combine with the anionic AMPSs, forming a new type of AMPSs/VIPS pair.[12] The equimolar pairing of AMPSs and VIPS is denoted as the AMPSs/VIPS. The strong ionic interaction between AMPSs and VIPS within or between the polymer chains of hydrogels acts as sacrificial secondary cross-linking, in addition to the primary chemical cross-linking originating from MBAA. In addition, the AAm monomer was copolymerized with AMPSs/VIPS to form the tough P(AMPSs/VIPS-co-AAm) hydrogel by shielding the repulsion between charged monomers[17–19] and forming numerous hydrogen bonds among AAm–AMPSs, AAm–AAm, and AAm–VIPS.[20] The synergistic effect of the dynamic ionic bonds and hydrogen bonds, which effectively dissipates the energy applied during deformation and restores the hydrogel to its original state, provides it with good mechanical toughness, high elongation, and excellent recovery characteristics. Furthermore, dissociation and transport of ionic salts from VIPS and AMPSs provide the hydrogel with high ionic conductivity.

3.2. Structure and morphology of P(AMPSs/VIPS-co-AAm) hydrogel

Polymerizable AMPSs/VIPS monomers were prepared by mixing equimolar anionic AMPSs and zwitterionic VIPS, as reported in a previous study.[6] The strong ionic interaction of cations of VIPS and anions of AMPSs allows AMPSs/VIPS pair of a melting temperature lower than 100 °C. The thermal properties of AMPSs, VIPS, and AMPSs/VIPS pair were investigated by differential scanning calorimetry (DSC), as shown in Fig. 2a. As the DCS curves indicate, the melting temperatures of AMPSs and VIPS were 153 and 79 °C, respectively. Interestingly, the melting temperature of AMPS/VIPS pair decreased to 65 °C, which is lower than that of individual monomers. This is due to the preferential interactions between imidazole cations of VIPS and sulfonate cations of AMPSs, as well as the reduced lattice energy of the AMPS/VIPS pair.[21]

The FTIR spectra of AMPSs, VIPS, AAm, and P(AMPSs/VIPS-co-AAm) hydrogels are shown in Fig. 2b. The absorption peak corresponding to each monomer can be observed. The characteristic peaks for AAm group were appeared at 3180 cm^{-1} (NH$_2$ symmetric stretching), 1614 cm^{-1} (NH bending), and 1673 cm^{-1} (C=O stretching vibration). The spectrum of AMPSs exhibited broad peaks at 3500–3000 cm^{-1} (NH and OH stretching), and sharp peak at 1662 (C=O stretching of amide I) and at 1608 cm^{-1} (N–H bending of amide II), respectively. Corresponding peak for asymmetric and symmetric stretching of sulfonic acid groups was shown at 1350–1060 cm^{-1}. The spectrum of VIPS includes CH in-plane deformed vibration of cyclic imidazole at 1173 cm^{-1}, the S=O stretching mode at 1205 and 1032 cm^{-1}, S=O stretching vibrations of the sulfate group at 1033 and 1179 cm^{-1}.[22] Even after photo-polymerization, the corresponding peaks of each monomer were observed, indicating that all monomers are well connected without loss. In addition, the –C=C– double bond peak disappeared near 980 cm^{-1} because of successful conversion to polymeric hydrogel chain (Fig. S1†).

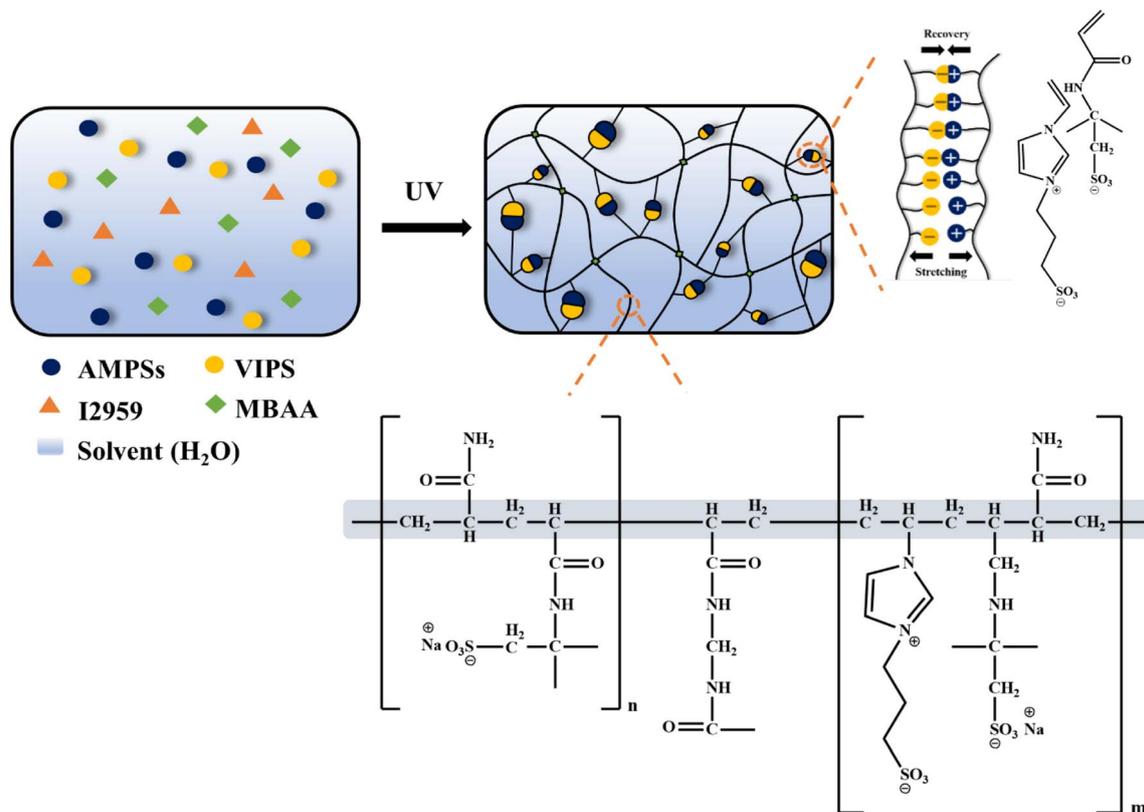Fig. 2c demonstrates the microstructure of the P(AMPSs/VIPS-co-AAm) hydrogel obtained by observing the cross-section

Fig. 1 Schematic illustration of the preparation and chemical interaction of the P(AMPSs/VIPS-*co*-AAm) hydrogel.

of the freeze-dried hydrogel samples by SEM. The SEM image clearly revealed that numerous pores exist inside the hydrogel, which might serve as an effective ion transport channel, thus providing excellent conductivity to the hydrogel.[23]

3.3. Mechanical properties of P(AMPSs/VIPS-*co*-AAm) hydrogel

Prior to evaluating the adhesion performance of the P(AMPSs/VIPS-*co*-AAm) hydrogel, the variation in the mechanical property was investigated according to the monomer composition of the hydrogel. First, tensile tests were conducted with monomer mole ratios of AMPSs/VIPS pairs to AAm in the range of 2 : 1 to 1 : 2 at a constant feed content of MBAA (0.15 mol% to monomer) (Fig. 3a). AAm incorporated into the hydrogel dramatically improved the mechanical property of the hydrogel despite that the hydrogel composed of AMPS/VIPS pairs lacked sufficient toughness to withstand the tensile-strain test (Fig. S2†). In addition, the increase in the AAm content incorporated in the hydrogel gradually increased the toughness while decreasing stretchability (Fig. 3a), decreased the fracture strain from 1313% to 1282% and 949%, and increased the tensile strength from 20 kPa to 40 kPa and 52 kPa. Further, Young's modulus of the hydrogel increased from 16.9 Pa to 52.4 Pa and 117.3 Pa (Fig. 3b). These trends are attributed to the enhanced internal cohesion of the hydrogel due to the formation of numerous hydrogen bonds between or within hydrogel polymer chains.[24] AAm groups of the hydrogel network can form strong hydrogen

bonding with adjacent AAm groups and amide groups of AMPSs. In addition, as shown in Fig. S3,† the P(AMPSs/VIPS-*co*-AAm) hydrogel has improved mechanical properties compared to the P(VIPS-*co*-AAm) hydrogel. The strong ionic interaction between AMPSs and VIPS within or between the hydrogel polymer chains acts as the secondary cross-linking point, in addition to the primary chemical cross-linking originating from MBAA. As a result, AMPSs/VIPS pairs of the hydrogel might additionally enhance the internal cohesion of the hydrogel.

The description for these possible mechanisms is detailed in Fig. 3c. Therefore, the internal cohesion of the hydrogel was greatly improved by various molecular interactions within polymer chains, which provide the hydrogel outstanding stretchability (1282% fracture strain) and moderate toughness (40 kPa tensile strength) when the AMPSs/VIPS : AAm ratio was 1 : 1 (mol mol^{-1}).

3.4. Adhesive properties of P(AMPSs/VIPS-*co*-AAm) hydrogel

In this study, the prepared P(AMPSs/VIPS-*co*-AAm) hydrogel has unique excellent adhesion properties on porcine skin (up to 217 N m^{-1}). It is known that the strength of the hydrogel's adhesion to the substrate is a synergistic result of the adhesive and cohesive properties of the hydrogel.[25,26] A 90° peeling test of the porcine skin was conducted to investigate the adhesive properties of the P(AMPSs/VIPS-*co*-AAm) hydrogel under different hydrogel compositions (Fig. 4). A 90° peeling test was then conducted, and the resulting peel strength–displacement
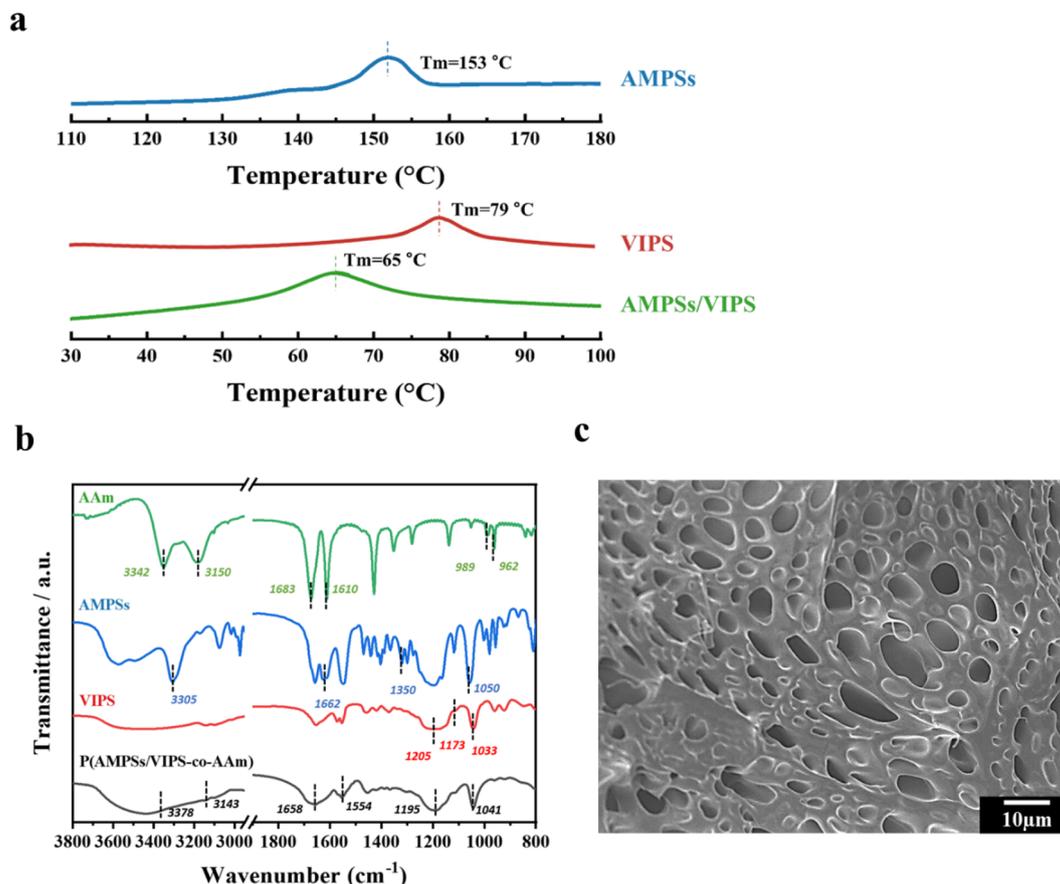
Fig. 2 (a) DSC curves of AMPSs, VIPS, and AMPSs/VIPS pair. (b) FTIR spectra of AAm, AMPSs, VIPS, and the P(AMPSs/VIPS-*co*-AAm) hydrogel. (c) SEM images showing the porous structure of the P(AMPSs/VIPS-*co*-AAm) hydrogel.

curves are shown in Fig. 4a. The average value obtained from the plateau region of the peel strength–displacement curve was used as the representative peel strength of each hydrogel. Similar to the tensile test (Fig. 3a), the effect of the monomer mole ratio of AMPSs/VIPS pairs to AAm (in the range of 2 : 1 to 1 : 2) on the hydrogel adhesion to porcine skin was investigated. Interestingly, when the AMPSs/VIPS : AAm ratio was 1 : 1 (mol mol^{-1}), the hydrogel had a maximum peel strength of 217 N m^{-1} (Fig. 4b and c). The adhesive property at the interface between the porcine skin and the hydrogel, which was derived from zwitterionic moiety, increased with increasing amount of AMPSs/VIPS in the hydrogel. In contrast, the internal cohesion of the hydrogel increased with increasing amount of AAm in the hydrogel, similar to the trend demonstrated by the mechanical property of the hydrogel (Fig. 3a). Therefore, at the AMPSs/VIPS : AAm mole ratio of 1 : 1, the highest peel strength of 217 N m^{-1} was obtained by the optimal balance between the interfacial adhesion and the internal cohesion of the hydrogel. Similar trends were observed in the experiment conducted with a varying amount of MBAA (0.1, 0.15, and 0.2 mol%) incorporated in the hydrogel at a fixed AMPSs/VIPSs : AAm ratio of 1 : 1 (mol mol^{-1}) (Fig. 4d). The resulting hydrogel showed the highest peeling strength through the optimal balance between the internal cohesive force and interfacial adhesive force when

0.15 mol% MBAA was used. In comparison, the P(AMPSs-*co*-AAm) hydrogel, prepared using AMPSs ionic monomers instead of AMPSs/VIPS pair, exhibited a low peel strength of 76 N m^{-1} on porcine skin (Fig. S4†). This result indicates that zwitterionic VIPS plays a key role in securing excellent interfacial adhesion to the porcine skin tissue as reported.[10] Imidazole N$^+$ group and sulfonate –SO$_3^-$ group of zwitterionic VIPS, which have a strong dipole moment, can interact with polar functional groups on the skin, such as –COOH, –NH$_2$, and –CONH, and –SH (Fig. 3c),[13,27] whereas only the anionic –SO$_3^-$ group of AMPSs can participate in interfacial adhesion. In addition, as mentioned above, the enhanced internal cohesion due to the strong ionic interaction between AMPSs and VIPS was advantageous for the P(AMPSs/VIPS-*co*-AAm) hydrogel to have the highest porcine skin adhesion. The resulting hydrogel exhibited excellent peeling force, reaching up to 217 N m^{-1} on porcine skin tissue at optimal composition.

The prepared P(AMPSs/VIPS-*co*-AAm) hydrogel revealed a robust bond to various polar substrates due to the interaction between the charged groups of AMPSs/VIPS pairs with other charged or polar moieties on the polar surface. The peel strength values for the P(AMPSs/VIPS-*co*-AAm) hydrogel on steel, glass, and acryl were 587, 191, and 100 N m^{-1}, respectively (Fig. S5†). In addition, the P(AMPSs/VIPS-*co*-AAm) hydrogel
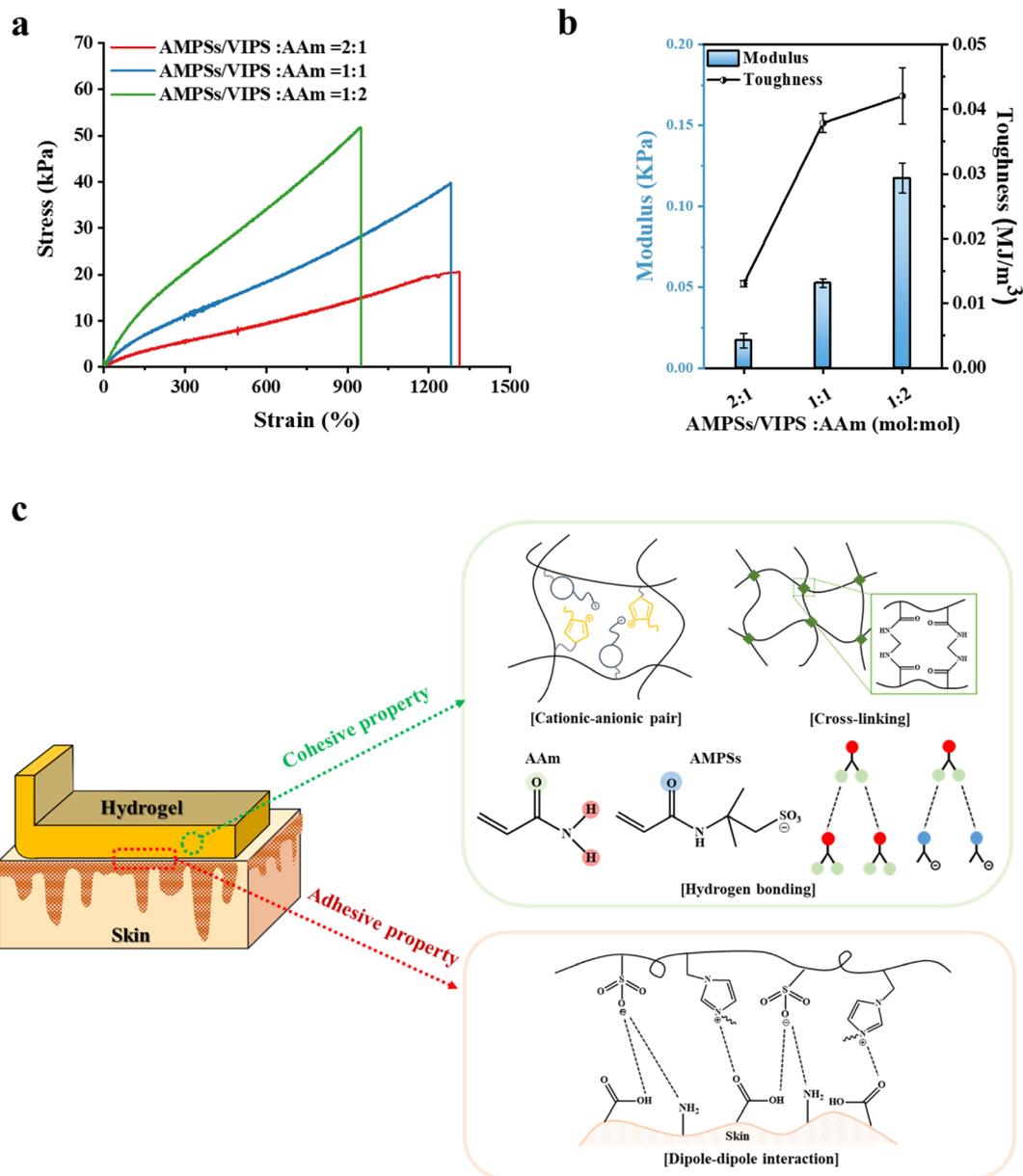
Fig. 3 (a) Tensile curves of the P(AMPSs/VIPS-*co*-AAm) hydrogel with different mole ratios of AAm and (b) the corresponding Young's modulus and toughness. (c) A representative mechanism associated with increased internal cohesive and interfacial adhesive properties.

itself firmly adhered to human skin for 30 minutes and detached clearly without residue or skin irritation upon removal (Fig. S6†).

As mentioned above, the prepared P(AMPSs/VIPS-*co*-AAm) hydrogel exhibited excellent adhesive strength of up to 217 N m^{-1} on porcine skin; this is attributed to the rational structure design and the optimal control of the hydrogel. Numerous existing studies evaluated the adhesive properties *via* a lab shear method. Therefore, it is difficult to directly compare the adhesive performance of the P(AMPSs/VIPS-*co*-AAm) hydrogel, as measured *via* a 90° peeling test, with that of other reported hydrogels.[8–10,13–15] For this reason, the adhesive properties of the P(AMPSs/VIPS-*co*-AAm) hydrogel were additionally evaluated using the lab shear test, as shown in Fig. 4e. The lab shear test

was conducted using assemblies with P(AMPSs/VIPS-*co*-AAm) hydrogels (15 mm × 15 mm × 3 mm) sandwiched between two porcine skin sheets (15 mm × 30 mm). Fig. 4f displays the representative force–displacement curve according to the variation of the AMPSs/VIPS : AAm monomer ratio of the hydrogel; the corresponding adhesive strength is shown in Fig. 4g. A similar trend was observed in the lap shear test when the AMPSs/VIPS : AAm mole ratio of the hydrogel was 1 : 1; here, the highest force of 6 N is required to separate two porcine skin sheets adhered to the hydrogel. The adhesive strength of the P(AMPSs/VIPS-*co*-AAm) hydrogel with the optimal formulations on porcine skin reached up to 26.9 kPa. The adhesive strength of the P(AMPSs/VIPS-*co*-AAm) hydrogel is a comparable to the highest value of previously reported zwitterion-based adhesive
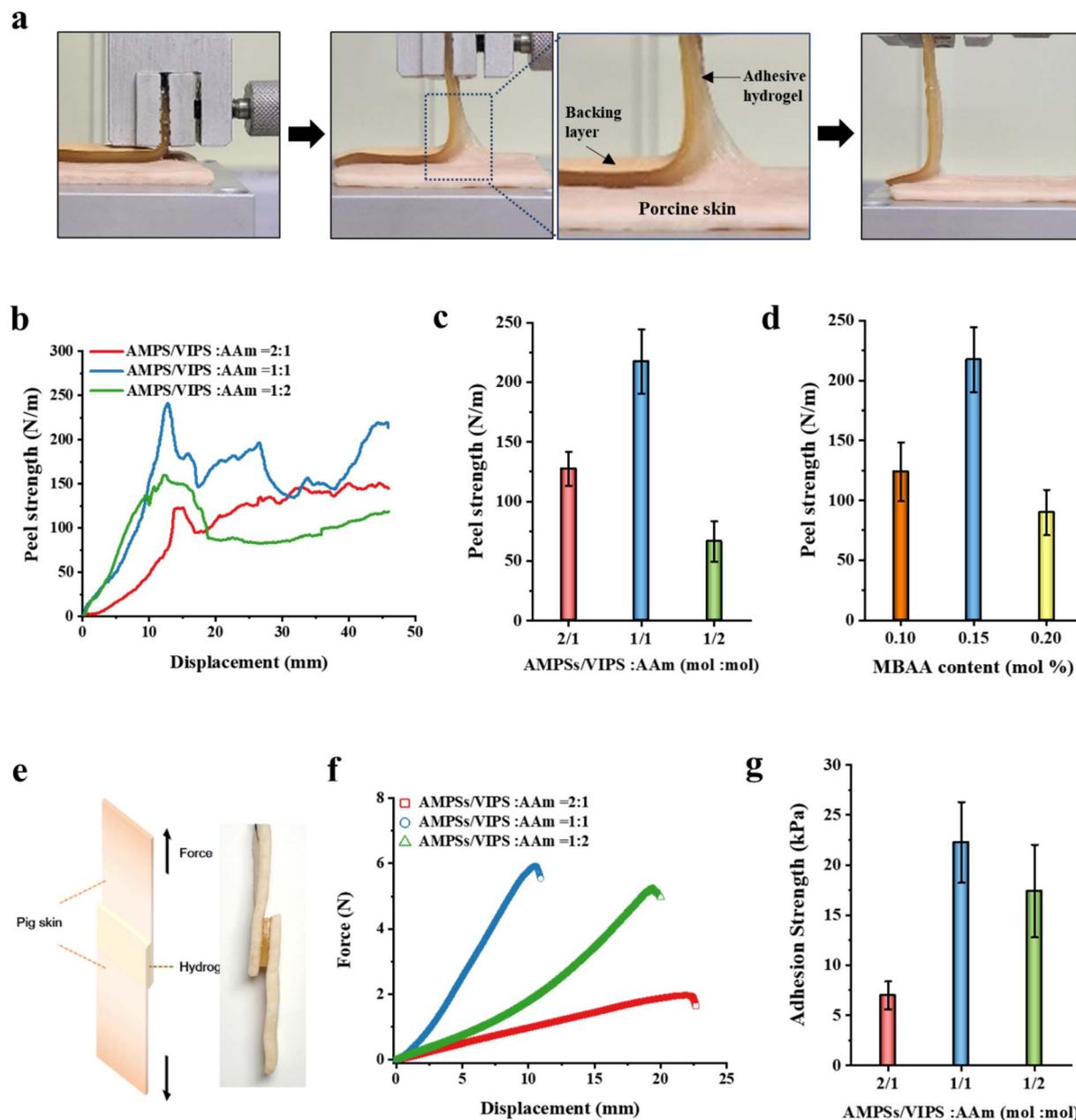
Fig. 4 (a) Images of the 90° peeling test conducted on the hydrogel adhered to the porcine skin at different peeling stages. (b) Schematic of the peeling test under different hydrogel compositions: AMPSs/VIPS : AAm ratio = 2 : 1, 1 : 1, and 1 : 2 (MBAA = 0.15 mol% relative to the monomer) and (c) corresponding peel strength results. (d) Peel strength of the P(AMPSs/VIPS-co-AAm) hydrogel with different MBAA contents. (e) Image of lap shear test of hydrogel sandwiched in two pig skin. (f) Force−displacement curves of lap shear test according to the different of monomer ratio AMPSs/VIPS : AAm ratio and (g) corresponding adhesive strength results.

hydrogels.[8–10,13–15] It is important to note that excellent skin adhesion (26.9 kPa) was obtained from all polymeric P(AMPSs/VIPS-co-AAm) hydrogels prepared by simple one-pot UV polymerization of the monomers without the incorporation of additives or fillers. In addition, these excellent adhesive properties were secured through a rational molecular design to improve the mechanical properties of the hydrogel while taking advantage of interfacial adhesiveness of zwitterion hydrogels.

3.5. Recovery properties and mechanical stabilities of P(AMPSs/VIPS-co-AAm) hydrogel

The strong ionic interaction between AMPSs and VIPS provides the hydrogel not only good mechanical toughness but also excellent recovery characteristics. Energy hysteresis and fatigue resistance of the P(AMPSs/VIPS-co-AAm) hydrogel were investigated by conducting tensile cyclic tests. Fig. 5a and b show the representative hysteresis curves of the hydrogel under different strains (100–1000% strain) during loading–unloading cycles.

The increase in strain from 100% to 1000% resulted in larger hysteresis loops, indicating the increased energy dissipation during loading. Measurements of ten continuous tensile cyclic loading–unloading tests to 500% strain (Fig. 5c) and the corresponding calculated hysteresis energy (Fig. 6d) were obtained. Interestingly, all hysteresis loops are overlaid at similar positions with very low hysteresis energies values of 3–4 kJ m^{-3}; this is lower than those of studies reporting low hysteresis energy (approximately 5 kJ m^{-3}).[28–30] The dynamic ionic bond between AMPSs and VIPS within or between hydrogel polymer chains serves as a secondary cross-linking point, effectively dissipating the energy applied during deformation and restoring the hydrogel to its original state after 10 loading–unloading cycles.

The enlarged graph for the first and second cycles clearly shows that the two curves start at almost the same position (Fig. S7†). This phenomenon is different from the recovery pattern of conventional adhesive hydrogels, which could not be restored to the original state because of the damaged internal network during the first cycle.[31] Numerous ionic interactions in the P(AMPSs/VIPS-co-AAm) hydrogel play a pivotal role in the reversible and rapid repair of the deteriorated internal structure of the hydrogel when the external force is removed. Moreover, the tensile stress of the loading step increased slightly as the

number of repeated cycles increased, as shown in the enlarged graph (inset of Fig. 5c). The increased toughness of the P(AMPSs/VIPS-co-AAm) hydrogel can be attributed to the rearrangement of the irregular segment of polymer chains during repeated stretching and recovery cycles, which results in the reversible formation of dynamic bonds such as ionic interaction and hydrogen bonding.[32] The excellent recovery, fatigue resistance, and network toughening properties effectively provide stable and robust mechanical properties for the long-term usage of the hydrogel.

3.6. Electrical and sensing properties of P(AMPSs/VIPS-co-AAm) hydrogel

The P(AMPSs/VIPS-co-AAm) hydrogel exhibits a high ionic conductivity due to the dissociation and transport of anionic AMPSs and zwitterionic salts. The ionic conductivity of the hydrogel was measured by a two-probe AC impedance method according to the variation in AMPSs/VIPS pair in the hydrogel; Fig. 6a shows the calculated ionic conductivities. A higher ionic conductivity was obtained by incorporating higher contents of AMPSs/VIPS in the hydrogel; the maximum conductivity of 0.62 S m^{-1} was observed at an AMPSs/VIPS : AAm ratio of 2 : 1 (mol mol^{-1}). At the AMPSs/VIPS : AAm ratio of 1 : 1 (mol mol^{-1}),
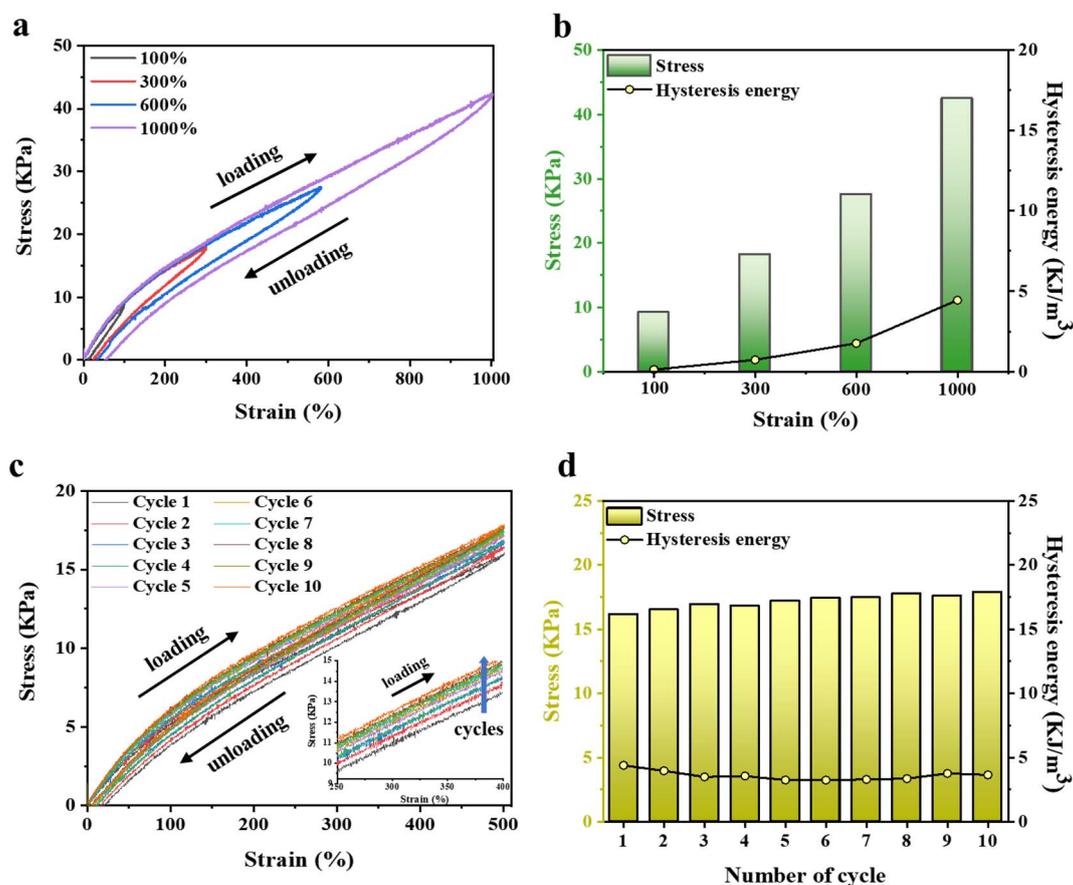

Fig. 5 (a)Tensile cyclic test of the P(AMPSs/VIPS-co-AAm) hydrogel with increasing strain (100%, 300%, 600%, 1000%) and (b) corresponding stress and hysteresis energy. (c) Ten successive tensile loading cycles at 500% strain without resting time. (d) The corresponding stress and hysteresis energy.
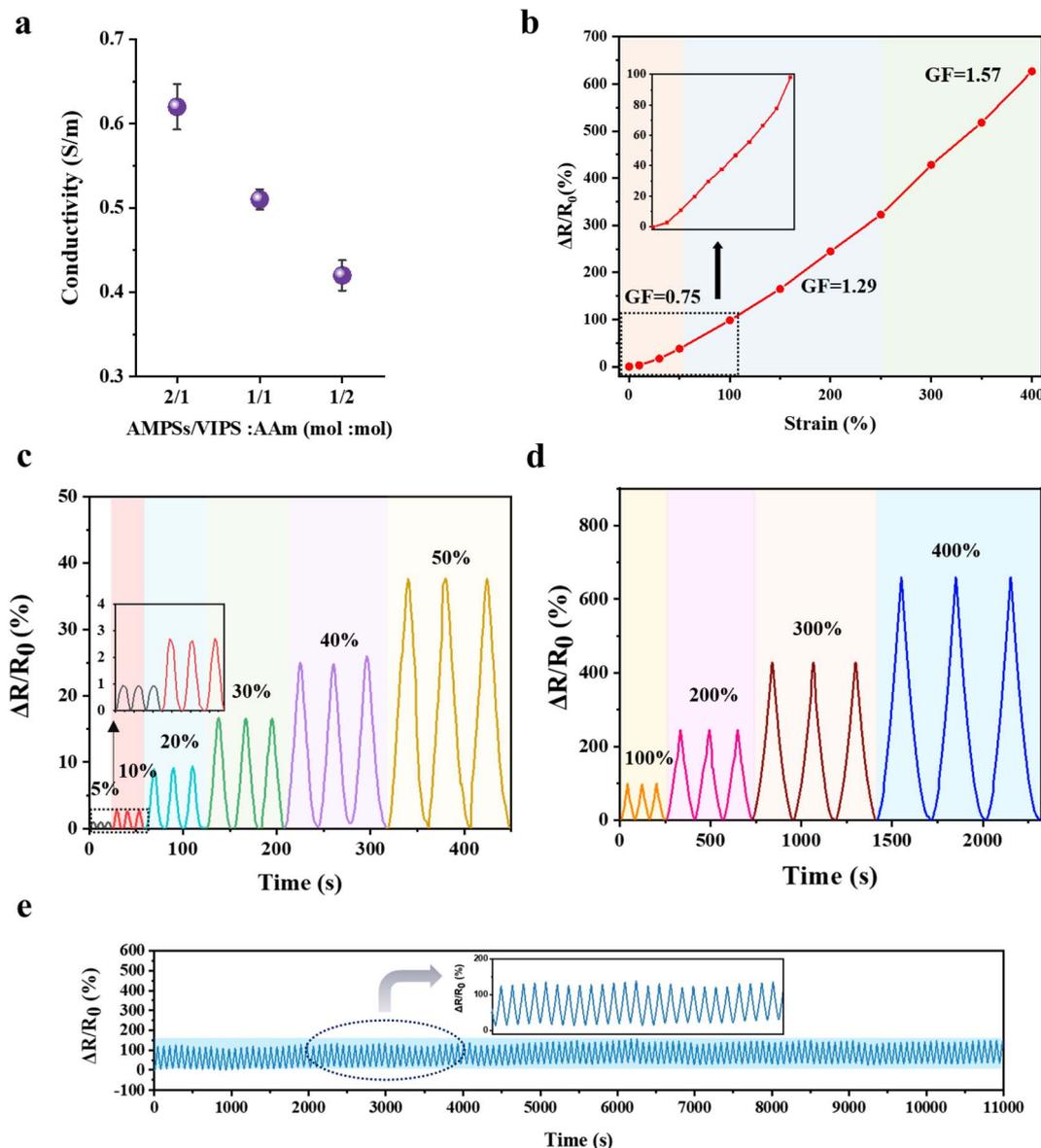
Fig. 6 (a) Ionic conductivity of the P(AMPSs/VIPS-co-AAm) hydrogel at varying AAm molar ratios. (b) The resistance change curves of the hydrogel under different strains (0–400%) and calculated gauge factor for the specific strain region. (c and d) Relative resistance curves for small strain (5–50%) and large strain (100–400%) ranges. (e) Repeated 300 loading–unloading cycles of the P(AMPSs/VIPS-co-AAm) hydrogel for testing long-term stability at 100% strain.

a conductivity of 0.51 S m^{-1} was selected as the optimal formulation because excellent skin adhesion and outstanding stretchability could be realized for application of the hydrogel as a strain sensor. The P(AMPSs/VIPS-co-AAm) hydrogel is sensitive to strain deformation. Fig. 6b indicates a linear increase in the resistance as the tensile strain of the hydrogel is increased from 0% to 400%; a resistance change of 626% is attained at 400% strain. The calculated gauge factor (GF) is specified for different strain regions. Importantly, the linear sensitivity of resistance to applied strain for the entire strain range (0–400%) provides a feasible working range of the sensor for detecting body motions.[33] Stable resistance change was observed for multiple deformations from a small strain region

(5–50%, Fig. 6c) to a large strain region (100–400%, Fig. 6d), indicating that the hydrogels possess good cyclic stability and repeatability. More importantly, the resistance changes for repeated 300 stretching cycles at 100% strain remain almost constant (Fig. 6e). This result might be related to the structural stability of the hydrogel, all component is incorporated into the hydrogel network and the formation of a stable ion channel through AMPSs/VIPS pairs.

As a wearable device, the strain sensor should be able to detect various ranges of strain induced by body motion[34] and needs to be firmly adhered to various body joint parts, such as a finger and an elbow, during the sensing process in order to precisely transmit the strain deformation to electric signals. As
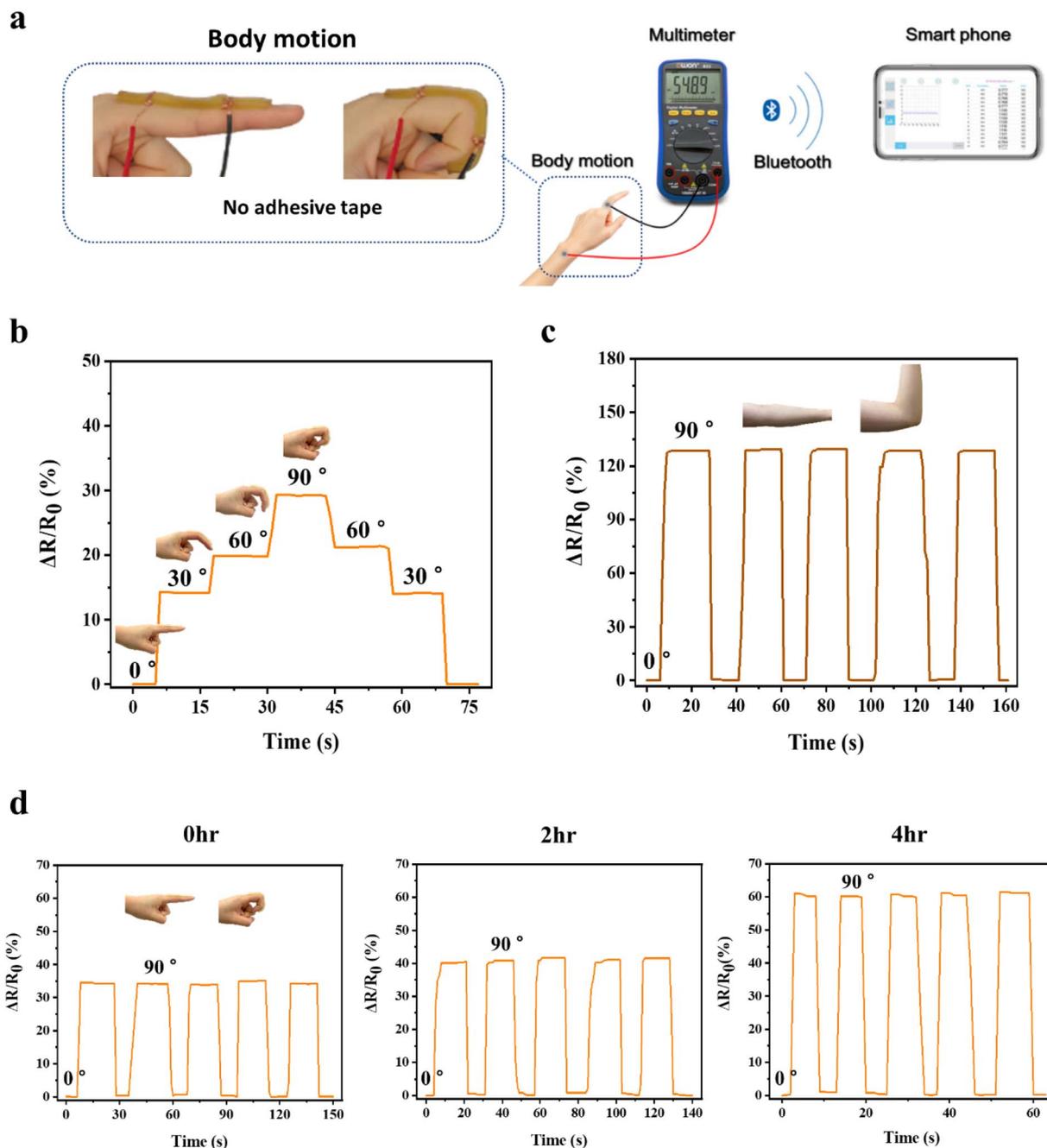
Fig. 7 (a) Real-time resistance-variation measurement using Bluetooth electronic devices. The real-time sensing of the P(AMPSs/VIPS-*co*-AAm) hydrogel in detecting human body motions: (b) finger bending at various angles (0° to 30°, 60°, and 90°) and (c) elbow bending (0° and 90°). (d) The relative resistance change upon repeated finger bending (0° and 90°) as a function of dehydration time.

adhesion of conventional conductive hydrogels to the skin was insufficient, they were attached to the skin using a commercial adhesive tape.[35] By contrast, the P(AMPSs/VIPS-*co*-AAm) hydrogels were directly adhered to different body parts, with only the copper wire connected to both ends of the hydrogel, and real-time resistance changes were measured by Bluetooth electronic devices (Fig. 7a). As shown in Fig. 7b, the hydrogel strain sensor could detect a subtle difference in the bending angle of the finger, ranging from 0° to 30°, 60°, and 90°. The resistance

change increased stepwise with an increase in the finger bending angle, and the electric signal immediately returned to its original value. The resistance change remained stable when the finger was held at a certain angle. In addition, the P(AMPSs/VIPS-*co*-AAm) hydrogel sensor accurately detected a large-scale body motion at the elbow (Fig. 7c).

For the practical application of a strain sensor, it is critical to maintain excellent adhesion to the skin for a long duration without a dramatic decrease in skin adhesion caused by

dehydration of the hydrogel. We investigated whether the P(AMPSs/VIPS-co-AAm) hydrogel can maintain the sensor performance under varying degrees of dehydration. We measured the 90° peel strength of the prepared hydrogel on the porcine skin exposed to ambient conditions (22 °C, 45% humidity) for 2, 4, and 6 hours. As shown in Fig. S8,† with prolonged exposure time to air, although the adhesion of the hydrogel slightly decreased from the initial high value of 217 N m^{-1}, excellent adhesion of 149 N m^{-1} on the porcine skin was maintained even after 6 hours. In addition, the water content and conductivity of the hydrogel decreased with increasing exposure time; nevertheless, appropriate levels for the application of the hydrogel as the strain sensor could be maintained even after 4 hours (Fig. S9 and S10†). Because of the advantageous properties mentioned above, the P(AMPSs/VIPS-co-AAm) hydrogels can serve as a strain sensor even after 4 hours of dehydration while retaining excellent resistance change upon repeated finger bending (Fig. 7d). The value of the relative resistance change ($\Delta R/R_0$) to the same body motion increased from the initial 35% to 60% after 4 hours; this might be attributed to the change in resistance and intrinsic properties of the hydrogel upon dehydration. The initial adhesion of the P(AMPSs-co-AAm) hydrogel was weak at a peel strength of 44 N m^{-1}, and we did not observe stable sensing characteristics as the hydrogel was detached from the skin during finger bending (Fig. S7d†). In addition, skin adhesion of the P(AMPSs-co-AAm) hydrogel further decreased as dehydration progressed, ultimately failing to adhere to the skin. These results represent the long-term stability of the sensing performance of the P(AMPSs/VIPS-co-AAm) hydrogel.

4. Conclusion

This study developed a facile preparation method for a skin adhesive hydrogel with high ionic conductivity, mechanical stability, and fatigue resistance. The multifunctional hydrogel was prepared by using all polymerizable AMPSs/VIPS pairs and acrylamide (AAm) to form an all-polymer network in the hydrogel. The P(AMPSs/VIPS-co-AAm) hydrogel thus prepared has several significant features. First, the adhesive strength to the porcine skin reached up to 26.9 kPa, which is comparable to the highest value of existing zwitterion-based hydrogels.[8–10,13–15] This outstanding adhesion capability was imparted by the hydrogel of the additive-free polymer prepared with a rational structural design and synergistic and optimal balance between interfacial adhesion and internal cohesion. Second, the hydrogel exhibited excellent fatigue resistance comparing to reported study.[28–30,36] And network toughening, electric stability even after multiple deformation, which can be attributed to the unity and stability of the hydrogel structure. Third, the P(AMPSs/VIPS-co-AAm) hydrogel retained excellent skin adhesion and strain sensitivity even after 4 hours of dehydration. These observations demonstrate the high feasibility for application of the hydrogel as a skin-adhesive, strain sensitive, reliable, and wearable sensing material for monitoring body motions over a long period. Since a wearable strain sensor can be used in extreme environments where sweat exists, it is important to

understand the effect of sweat on sensing performance and skin adhesion of hydrogel, and secure a stable sensing performance in such extreme environments for practical purposes. As a result, more efforts should be devoted to research to settle down these issues in the future.

Conflicts of interest

There are no conflicts to declare.

Acknowledgements

References

1 P. Rahmani and A. Shojaei, *Adv. Colloid Interface Sci.*, 2021, **298**, 102553.

2 H. Yuk, T. Zhang, S. Lin, G. A. Parada and X. Zhao, *Nat. Mater.*, 2016, **15**, 190–196.

3 Y. Chevalier, Y. Storet, S. Pourchet and P. Le Perchec, *Langmuir*, 1991, **7**, 848–853.

4 H. Jung, M. K. Kim, J. Y. Lee, S. W. Choi and J. Kim, *Adv. Funct. Mater.*, 2020, **30**, 1–10.

5 Y. Chen, C. Zhang, R. Yin, A. Yin, Q. Feng, F. Liu, J. Shao, T. Su, H. Wang, G. Chen and W. Zhao, *Chem. Eng. J.*, 2022, **449**, 137907.

6 Y. Yu, F. Xie, X. Gao and L. Zheng, *Soft Matter*, 2021, **17**, 4352–4362.

7 D. Zhang, Y. Tang, Y. Zhang, F. Yang, Y. Liu, X. Wang, J. Yang, X. Gong and J. Zheng, *J. Mater. Chem. A*, 2020, **8**, 20474–20485.

8 X. Pei, H. Zhang, Y. Zhou, L. Zhou and J. Fu, *Mater. Horiz.*, 2020, **7**, 1872–1882.

9 B. Yang and W. Yuan, *ACS Appl. Mater. Interfaces*, 2019, **11**, 40620–40628.

10 L. Wang, G. Gao, Y. Zhou, T. Xu, J. Chen, R. Wang, R. Zhang and J. Fu, *ACS Appl. Mater. Interfaces*, 2019, **11**, 3506–3515.

11 T. Sakai, T. Matsunaga, Y. Yamamoto, C. Ito, R. Yoshida, S. Suzuki, N. Sasaki, M. Shibayama and U. Chung, *Macromolecules* 2008, 5379–5384.

12 T. Zhou, X. Gao, B. Dong, N. Sun and L. Zheng, *J. Mater. Chem. A*, 2016, **4**, 1112–1118.

13 Y. Huangfu, S. Li, L. Deng, J. Zhang, P. Huang, Z. Feng, D. Kong, W. Wang and A. Dong, *ACS Appl. Mater. Interfaces*, 2021, **13**, 59695–59707.

14 Z. Wang, J. Chen, L. Wang, G. Gao, Y. Zhou, R. Wang, T. Xu, J. Yin and J. Fu, *J. Mater. Chem. B*, 2019, **7**, 24–29.

15 J. Wang, L. Wang, C. Wu, X. Pei, Y. Cong, R. Zhang and J. Fu, *ACS Appl. Mater. Interfaces*, 2021, **12**, 46816–46826.

16 F. Lind, L. Rebollar, P. Bengani-Lutz, A. Asatekin and M. J. Panzer, *Chem. Mater.*, 2016, **28**, 8480–8483.

17 L. Wang, G. Shan and P. Pan, *Soft Matter*, 2014, **10**, 3850–3856.

18 S. Heo, H. Seo, C. Song, S. Shin and K. Kwon, *J. Mater. Chem. C*, 2021, **9**, 16778–16787.

19 H.-S. Seo, J.-Y. Bae, K. Kwon and S. Shin, *Polymers*, 2022, **14**, 2547.

20 E. Su, M. Yurtsever and O. Okay, *Macromolecules*, 2019, **52**, 3257–3267.

21 X. Gao, F. Lu, L. Shi, H. Jia, H. Gao and L. Zheng, *ACS Appl. Mater. Interfaces*, 2013, **5**, 13312–13317.

22 F. Lu, X. Gao, A. Wu, N. Sun, L. Shi and L. Zheng, *J. Phys. Chem. C*, 2017, **121**, 17756–17763.

23 D. S. Silvaraj, S. Bashir, M. Hina, J. Iqbal, S. Gunalan, S. Ramesh and K. Ramesh, *J. Energy Storage*, 2021, **35**, 102320.

24 Y. Gao, F. Jia and G. Gao, *Chem. Eng. J.*, 2019, **375**, 121915.

25 C. R. Matos-Pérez, J. D. White and J. J. Wilker, *J. Am. Chem. Soc.*, 2012, **134**, 9498–9505.

26 J. Xu, Z. Fan, L. Duan and G. Gao, *Polym. Chem.*, 2018, **9**, 2617–2624.

27 W. Zhang, B. Wu, S. Sun and P. Wu, *Nat. Commun.*, 2021, **12**(1), 4082.

28 W. J. Zheng, Y. Gao, X. X. Fan, X. F. Cui, W. Zou, D. Zheng, J. Yan and B. Li, *Macromol. Mater. Eng.*, 2018, **303**, 1–7.

29 K. Xu, K. Shen, J. Yu, Y. Yang, Y. Wei, P. Lin, Q. Zhang, C. Xiao, Y. Zhang and Y. Cheng, *Chem. Mater.*, 2022, **34**, 3311–3322.

30 X. Su, S. Mahalingam, M. Edirisinghe and B. Chen, *ACS Appl. Mater. Interfaces*, 2017, **9**, 22223–22234.

31 Q. Jiao, L. Cao, Z. Zhao, H. Zhang, J. Li and Y. Wei, *Biomacromolecules*, 2021, **22**, 1220–1230.

32 X. Zhang, R. Zhang, S. Wu, Y. Sun, H. Yang and B. Lin, *New J. Chem.*, 2020, **44**, 9903–9911.

33 Z. Wang, J. Chen, Y. Cong, H. Zhang, T. Xu, L. Nie and J. Fu, *Chem. Mater.*, 2018, **30**, 8062–8069.

34 D. Zhang, B. Ren, Y. Zhang, L. Xu, Q. Huang, Y. He, X. Li, J. Wu, J. Yang, Q. Chen, Y. Chang and J. Zheng, *J. Mater. Chem. B*, 2020, **8**, 3171–3191.

35 H. Sun, Y. Zhao, C. Wang, K. Zhou, C. Yan, G. Zheng, J. Huang, K. Dai, C. Liu and C. Shen, *Nano Energy*, 2020, **76**, 105035.

36 X. Fan, S. Pan, M. Xia, J. Yin, H. Li, Z. Sun, Y. Zhan and Y. Zhang, *Mater. Res. Bull.*, 2022, **146**, 111627.